Copyright 2004 Tech Science Press

Scaled Boundary Finite-Element Solutions for Singular Stress Fields in Multi-Material Wedges

Chongmin Song[1]

Summary

The singular stress fields around the vertices of multi-material wedges with arbitrary geometries and material combinations are analyzed by the scaled boundary finite-element method. The complete singular stress fields including: orders of singularity; stress intensity factors; T-stresses and higher-order terms in the asymptotic expansions; power-logarithmic singularities and angular distributions of stresses, are obtained in a single method. The singular functions are represented analytically and are not evaluated close to the singular point in determining the stress intensity factors, leading to high accuracy and simplicity.

Introduction

The novel scaled boundary finite-element method [1, 2] is applied to analyze the stress fields in multi-material wedges. The boundary of a multi-material wedge, excluding the straight surfaces forming the vertex, is discretized with elements. In the circumferential directions parallel to the boundary, where the response varies smoothly, the solution is discretized based on the standard finite element formulation. In the radial direction passing through the vertex, where the stress singularities occur, an analytical solution is obtained without any *a priori* assumptions. The semi-analytical solution of the complete stress field includes not only singular stress and T-stress terms but also higher-order terms. The transition between power and power-logarithmic singularities is accurately represented.

Summary of The Scaled Boundary Finite-Element Method

A so-called scaling centre O is chosen in a zone from which the total boundary must be visible (Fig. 1a). The boundary S is discretized with line elements. The geometry of an element is interpolated using the mapping functions $[N(\eta)]$ in the local coordinate η and the nodal coordinates $\{x\}$, $\{y\}$. The domain V is described by scaling the boundary with a dimensionless radial coordinate ξ pointing away from the scaling centre O $(\hat{x}_0, \hat{y}_0)$. $\xi = 0$ at O and $\xi = 1$ on the boundary is chosen. A point $(\hat{x}, \hat{y})$ inside the domain is expressed as

$$\hat{x}(\xi,\eta) = \hat{x}_0 + \xi[N(\eta)]\{x\}; \qquad \hat{y}(\xi,\eta) = \hat{y}_0 + \xi[N(\eta)]\{y\} \tag{1}$$

ξ, η are called the *scaled boundary coordinates* in two dimensions. They resemble the polar coordinates $\hat{r}$ and θ. The boundary S in Fig. 1a is transformed to a circle described by a constant radial coordinate $\xi = 1$ (Fig. 1b). The domain V is specified by $0 \le \xi \le 1$. When the origin of a polar coordinate system $(\hat{r}, \theta)$ coincides with the scaling centre (Fig. 1b)

$$\hat{r}(\xi,\eta) = \xi r(\eta) = \xi\sqrt{x^2(\eta)+y^2(\eta)}; \qquad \theta(\eta) = \arctan(y(\eta)/x(\eta)) \tag{2}$$

[1]School of Civil and Environmental Engineering, University of New South Wales, Sydney, NSW 2052, Australia

Copyright 2004 Tech Science Press

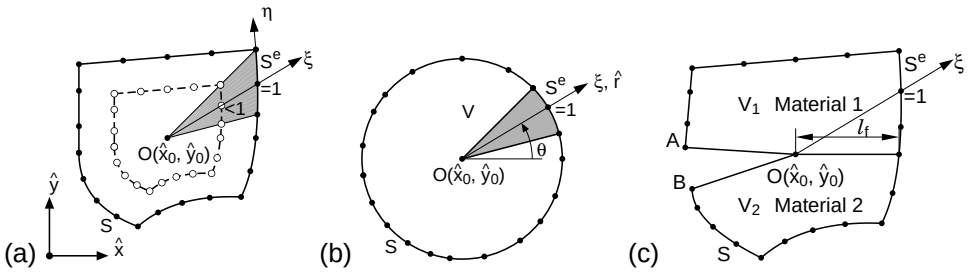

Figure 1: Scaled boundary coordinates: (a) scaling centre O, radial coordinate ξ and boundary discretization; (b) transformed domain; (c) representation of bi-material wedge.

applies. Multi-material wedges, as shown in Fig. 1c with a bi-material wedge as an example, are conveniently defined by constant values of the scaled boundary coordinates when the scaling centre O is chosen at the vertex. The two straight edges passing through the scaling centre are defined by constant circumferential coordinates η and are not discretized. Along the radial lines passing through the scaling centre O and a node on the boundary (Fig. 1) the nodal displacement functions $\{u(\xi)\}$ are introduced. The displacements at a point (ξ, η) are interpolated from the nodal functions

$$\{u(\xi,\eta)\} = [N^u(\eta)]\{u(\xi)\} = [N_1(\eta)[I],\ N_2(\eta)[I],\ldots]\{u(\xi)\} \tag{3}$$

The strains are expressed in the scaled boundary coordinates as (the argument η in $[B^1(\eta)]$ and $[B^2(\eta)]$ is omitted for simplicity)

$$\{\varepsilon(\xi,\eta)\} = [B^1]\{u(\xi)\}_{,\xi} + \frac{1}{\xi}[B^2]\{u(\xi)\} \tag{4}$$

$$[B^1] = \frac{1}{|J|}\begin{bmatrix} y_{,\eta} & 0 \\ 0 & -x_{,\eta} \\ -x_{,\eta} & y_{,\eta} \end{bmatrix}[N^u]; \quad [B^2] = \frac{1}{|J|}\begin{bmatrix} -y & 0 \\ 0 & x \\ x & -y \end{bmatrix}[N^u]_{,\eta}; \quad |J| = xy_{,\eta} - yx_{,\eta} \tag{5}$$

The element coefficient matrices are written as

$$\begin{aligned} [E^0] &= \int_{-1}^{+1}[B^1]^T[D][B^1]|J|\mathrm{d}\eta; \qquad [E^1] = \int_{-1}^{+1}[B^2]^T[D][B^1]|J|\mathrm{d}\eta; \\ [E^2] &= \int_{-1}^{+1}[B^2]^T[D][B^2]|J|\mathrm{d}\eta \end{aligned} \tag{6}$$

where the elasticity matrix $[D]$ can be that of any general anisotropic material. The coefficient matrices on the total boundary are obtained by assembling the element coefficient matrices in the same way as in the finite element method (The same symbols are used for simplicity). The scaled boundary finite-element equation in displacement is written as

$$[E^0]\xi^2\{u(\xi)\}_{,\xi\xi} + ([E^0] - [E^1] + [E^1]^T)\xi\{u(\xi)\}_{,\xi} - [E^2]\{u(\xi)\} = 0 \tag{7}$$

Decomposing the Hamiltonian matrix formed by the coefficient matrices

$$[Z] = \begin{bmatrix} [E^0]^{-1}[E^1]^T & -[E^0]^{-1} \\ -[E^2] + [E^1][E^0]^{-1}[E^1]^T & -[E^1][E^0]^{-1} \end{bmatrix} \tag{8}$$

Copyright 2004 Tech Science Press

into a block-diagonal real Schur form using the transformation matrix $[\Psi]$ leads to

$$[\Psi]^{-1}[Z][\Psi] = [S] = \text{diag}\left(\text{diag}([S_{\text{n}ii}]),\ \begin{bmatrix}0 & [I]\\ 0 & 0\end{bmatrix},\ \text{diag}([S_{\text{p}ii}])\right) \tag{9}$$

The diagonal blocks of the matrix $[S]$ are arranged to have all the diagonal entries of $[S_{\text{n}}]$ and $[S_{\text{p}}]$ being negative and positive, respectively. In addition, the eigenvalues of all the square diagonal blocks $[S_{\text{n}ii}]$ and $[S_{\text{p}ii}]$ are disjoint. $[\Psi]$ is partitioned conformably to $[S]$ as

$$[\Psi] = \begin{bmatrix} [\Psi_{\text{u}1}] & [\Psi_{\text{u}2}] & [\Psi_{\text{u}3}] & [\Psi_{\text{u}4}] \\ [\Psi_{\text{q}1}] & 0 & [\Psi_{\text{q}3}] & [\Psi_{\text{q}4}] \end{bmatrix} \tag{10}$$

The solution for a multi-material wedge with $0 \le \xi \le 1$ (Fig. 1c) is expressed as

$$\{u(\xi)\} = [\Psi_{\text{u}1}]\xi^{-[S_{\text{n}}]}\{c_1\} + [\Psi_{\text{u}2}]\{c_2\} \tag{11}$$

The integration constants $\{c_1\}$ and $\{c_2\}$ are determined from the displacements on the boundary $\{u(\xi = 1)\}$. The stresses are written as (omitting the subscript 1 in $\{c_1\}$)

$$\{\sigma(\xi,\eta)\} = [\Psi_\sigma(\eta)]\xi^{-1}\xi^{-[S_{\text{n}}]}\{c\} = \sum_i [\Psi_{\sigma i}(\eta)]\xi^{-1}\xi^{-[S_{\text{n}ii}]}\{c_i\} \tag{12}$$

$$\text{with} \qquad [\Psi_\sigma(\eta)] = [D]\left(-[B^1(\eta)][\Psi_{\text{u}1}][S_{\text{n}}] + [B^2(\eta)][\Psi_{\text{u}1}]\right) \tag{13}$$

In the radial direction, the stress field is described analytically by the matrix power function of dimensionless radial coordinate ξ. In the circumferential direction, it is approximated by piecewise smooth functions $[\Psi_\sigma(\eta)]$ of the local coordinate η. $[\Psi_\sigma(\eta)]$ can be evaluated at given values of η, or angle θ (Eq. (2)), by using the standard finite element techniques.

Singular Stress Fields

The stress solution (Eq. (12)) is in the form of an asymptotic expansion, whose coefficients can be determined by matching it with Eq. (12) term-by-term at $\xi = 1$. The stress term is singular when the real part of an eigenvalue λ_i of $[S_{\text{n}}]$ satisfies $0 > \lambda_{i\text{R}} > -1$. The stress term in Eq. (12) for a real eigenvalue with an independent eigenvector is written as

$$\{\sigma_i(\xi,\eta)\} = c_i\xi^{-\lambda_i-1}\{\Psi_{\sigma i}(\eta)\} \tag{14}$$

For a pair of complex conjugate denoted as $\lambda_i = \lambda_{i\text{R}} + \text{i}\lambda_{i\text{I}}$, $\bar{\lambda}_i = \lambda_{i\text{R}} - \text{i}\lambda_{i\text{I}}$, the stress is

$$\{\sigma_i(\xi,\eta)\} = \xi^{-\lambda_{i\text{R}}-1}[\Psi_{\sigma i}(\eta)]\begin{bmatrix}\cos(\lambda_{i\text{I}}\ln\xi) & -\sin(\lambda_{i\text{I}}\ln\xi)\\ \sin(\lambda_{i\text{I}}\ln\xi) & \cos(\lambda_{i\text{I}}\ln\xi)\end{bmatrix}\{c_i\} \tag{15}$$

as in the asymptotic expansions for cracks on bi-material interfaces [3]. The stress-intensity factor is determined by the singular stresses $\{\sigma^{(s)}\}$ calculated at ($\xi = 1$, $\eta(\theta = 0)$)

$$\begin{Bmatrix} K_I \\ K_{II} \end{Bmatrix} = \sqrt{2\pi}{l_f}^{\lambda_{s\text{R}}+1}\begin{bmatrix} \cos\left(-\lambda_{i\text{I}}\ln\frac{l_f}{L}\right) & \sin\left(-\lambda_{i\text{I}}\ln\frac{l_f}{L}\right) \\ -\sin\left(-\lambda_{i\text{I}}\ln\frac{l_f}{L}\right) & \cos\left(-\lambda_{i\text{I}}\ln\frac{l_f}{L}\right)\end{bmatrix}\begin{Bmatrix}\sigma_{yy}^{(s)}\\ \sigma_{xy}^{(s)}\end{Bmatrix} \tag{16}$$

Copyright 2004 Tech Science Press

where l_f is the distance from the crack tip to the boundary in its front (Fig. 1c). L is a characteristic length. When two eigenvalues correspond to one independent eigenvector, the diagonal block and the stresses are formulated as ($a \neq 0$ is a real number)

$$[S_{\mathrm{n}ii}] = \begin{bmatrix} \lambda_i & a \\ 0 & \lambda_i \end{bmatrix}; \quad \{\sigma_i(\xi,\eta)\} = \xi^{-\lambda_i - 1}[\Psi_{\sigma i}] \begin{bmatrix} 1 & -a\ln\xi \\ 0 & 1 \end{bmatrix} \{c_i\} \tag{17}$$

A logarithmic function appears in the stress solution.

Numerical Examples

An edge-cracked rectangular plate in plane strain is shown in Fig. 2. The crack length is $a = b/4$ The material is isotropic with the Young's modulus E and Poisson's ratio $\nu = 0.25$. The boundary of the plate is discretized with 4-node elements. The initial mesh of 10 elements is shown in Fig. 2. The coefficients of the first 5 terms a_i^1, $i = 1,2,\ldots,5$ of the asymptotic expansion [4] are calculated and shown in Table 1. They converge as the mesh is refined and are in good agreement with the results in Refs. [4,5].

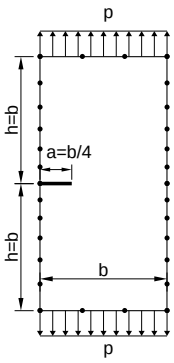

Figure 2: Edge-cracked rectangular plate.

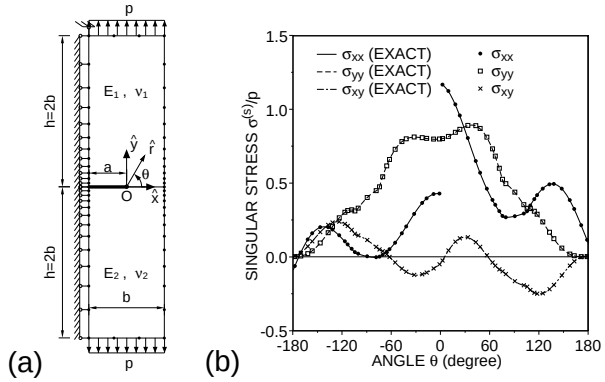

Figure 3: Central-cracked bi-material plate: (a) geometry; (b) singular stress term on boundary.

A central-cracked bi-material plate with the crack length $a/b = 0.5$ in plane strain is examined. Due to symmetry, only half of the plate is discretized with 18 4-node elements (Fig. 3a). The stress-intensity factors and T-stress obtained for the ratios of Young's moduli $E_1/E_2 = 1,5$ and 10 and contant Poisson's ratio $\nu_1 = \nu_2 = 0.3$. The characteristic length $L = 2a$ (Eq. (16)) is chosen. The stress-intensity factors K_I, K_{II} and $K_0 = (K_I^2 + K_{II}^2)^{1/2}$ are normalized by $p\sqrt{\pi a}$ and shown in Table 2. The T-stress is evaluated at the side of Material 1 (at $\theta = 0^+$) and compared with the results in Ref. [6]. The exact solution for the distribution of the singular stress term [6] on the boundary of the plate is calculated for $E_1/E_2 = 10$ with the values of K_I and K_{II} given in Table 2. It is plotted in Fig. 3b as continuous lines. Discrete values at Gauss points obtained using the scaled boundary finite-element method are plotted in the same figure. The two sets of results are indistinguishable.

A crack along the interface of two anisotropic half-planes in plane strain condition is

Copyright 2004 Tech Science Press

Table 1: Coefficients a_i^1 of the asymptotic expansion for edge-cracked rectangle plate.

	Number of Elements			Ref. [5]	Ref. [4]
	10	20	30		
$a_1^1/(p\sqrt{a})$	1.05615	1.05955	1.05959	1.0597	1.0585
a_2^1/p	−0.14952	−0.15058	−0.15059	−0.1503	−0.1513
$a_3^1/(p/\sqrt{a})$	0.08021	0.07945	0.07944	0.082	0.0815
$a_4^1/(p/a)$	−0.04821	−0.04760	−0.04761	−0.04856	−0.0478
$a_5^1(p/\sqrt[3]{a})$	0.00595	0.00559	0.00562		0.0055

Table 2: Stress intensity factors and T-stress of central-cracked bi-material plate.

E_1/E_2	$K_I/(p\sqrt{\pi a})$	$K_{II}/(p\sqrt{\pi a})$	$K_0/(p\sqrt{\pi a})$	$T\sqrt{\pi a}/K_0$	$T\sqrt{\pi a}/K_0$ ([6])
1	1.189	0.000	1.189	−1.060	−1.07
5	1.148	−0.104	1.153	−0.379	−0.39
10	1.123	−0.123	1.130	−0.216	−0.23

shown in Fig. 4. A force P is applied perpendicularly on the upper crack face at a distance a from the crack tip. The material properties are: $E_{11} = 0.09852$, $E_{22} = 0.58140$, $G_{12} = 0.07813$, $\nu_{12} = 0.0857$ for material 1 and $E_{11} = 0.06452$, $E_{22} = 1.70358$, $G_{12} = 0.08696$, $\nu_{12} = 0.02129$ for material 2 [7]. A circular boundary, discretized with 12 cubic elements, of radius a with its centre at the crack tip (Fig. 4a) is introduced. The exact order of stress singularity $1 + \lambda = 0.5 + \mathrm{i}0.012$ is obtained. The angular distribution of stresses at $\hat{r} = 0.01a$ is very close to the that of the analytical solution [7] as shown in Fig. 4b.

An isotropic bi-material wedge in plane strain with Young's moduli $E_1/E_2 = 10$ and Poisson's ratios $\nu_1 = \nu_2 = 0.2$ is shown in Fig. 5. At the opening angle $\theta_1 = \theta_2 = 138.7719^\circ$, a logarithmic term occurs in the solution with the order of singularity $\lambda + 1 = 0.3214741102$ (Ref. [8]). The boundary of the plate is discretized with 18 cubic elements. The diagonal block in $[S_\mathrm{n}]$ (Eq. (9)) leading to stress singularities is denoted as $[s]$. Its diagonal terms $s_{11} = -0.67879$ and $s_{22} = -0.67826$, are close to the exact eigenvalue of $\lambda = -0.67853$. The off-diagonal term $s_{12} = 0.33465$ is three orders of magnitude larger than the difference between s_{11} and s_{22}. The normalized stress components σ_{yy}/p and σ_{xy}/p are multiplied with $(\hat{r}/b)^{\lambda+1} = (\hat{r}/b)^{0.32147}$ and plotted versus $\log(\hat{r}/b)$ in Fig. 5b. A finite element analysis is performed using 10758 4-node quadrilateral elements with 10861 nodes to verify the results. Within a distance $\hat{r} = 0.01b$ from the notch tip, the curves become inclined straight lines. This demonstrates that the strongest singularity around the notch tip is $\hat{r}^{0.32147}\log\hat{r}$.

Reference

1. Song, Ch., Wolf, J. P. (1997): "The scaled boundary finite-element method – alias consistent infinitesimal finite-element cell method – for elastodynamics", *Computer Methods in Applied Mechanics and Engineering*, Vol. 147, pp. 329–355.
2. Song, Ch., Wolf, J. P. (2002): "Semi-analytical representation of stress singularity as occurring in cracks in anisotropic multi-materials with the scaled boundary finite-element method", *Computers & Structures*, Vol. 80, pp. 183–197.

Copyright 2004 Tech Science Press

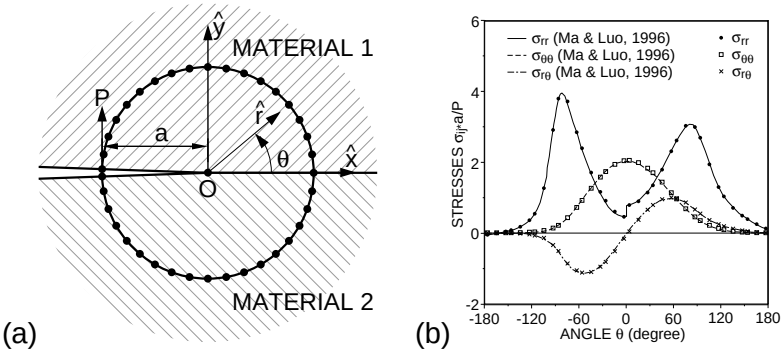

Figure 4: Interface crack in anisotropic bi-material full-plane: (a) geometry; (b) angular distribution of stresses at $\hat{r} = 0.01a$.

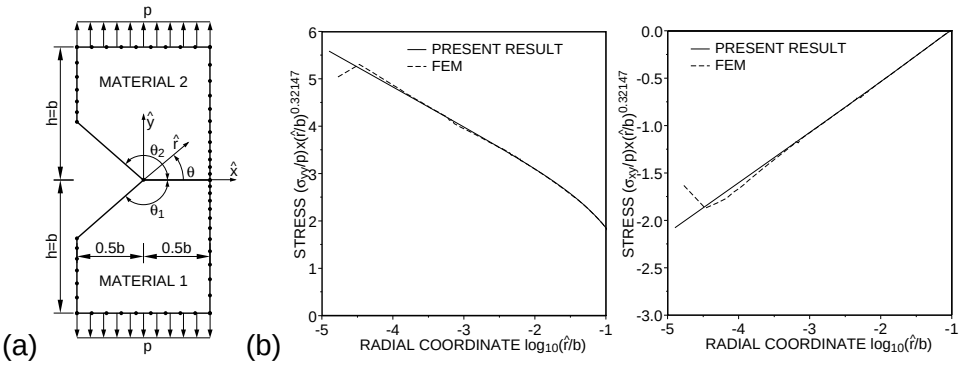

Figure 5: Notched bi-material plate: (a) geometry; (b) stresses on material interface.

3. Rice, J. R. (1988): "Elastic fracture mechanics concepts for interfacial cracks", *Journal of Applied Mechanics, ASME*, Vol. 55, pp.98–103.
4. Karihaloo, B. L., Q. Z. (2001): "Accurate determination of the coefficients of elastic crack tip asymptotic field by a hybrid crack element with *p*-adaptivity", *Engineering Fracture Mechanics*, Vol. 68, pp. 1609–1630.
5. Fett, T. (1998): "T-stresses in rectangular plates and circular disks", *Engineering Fracture Mechanics* Vol. 60, pp. 631–652.
6. Sladek, J., Sladek, V. (1997): "Evaluations of the *T*-stress for interface cracks by the boundary element method", *Engineering Fracture Mechanics* Vol. 56, pp. 813–825.
7. Ma, C. C., Luo, J. J. (1996): "Plane solutions of interface cracks in anisotropic dissimilar media", *Journal of Engineering Mechanics, ASCE*. Vol. 122, pp. 30–38.
8. Gadi, K. S., Josepha, P. F., Zhang, N. S., Kaya, A. C. (2000): "Thermally induced logarithmic stress singularities in a composite wedge and other anomalies", *Engineering Fracture Mechanics.* Vol.65, pp. 645–664.